www.sciencemag.org/cgi/content/full/1158088/DC1

Supporting Online Material for

The Metamorphosis of Supernova SN 2008D/XRF 080109: A Link Between Supernovae and GRBs/Hypernovae

Paolo A. Mazzali,* Stefano Valenti, Massimo Della Valle, Guido Chincarini, Daniel N. Sauer, Stefano Benetti, Elena Pian, Tsvi Piran, Valerio D'Elia, Nancy Elias-Rosa, Raffaella Margutti, Francesco Pasotti, L. Angelo Antonelli, Filomena Bufano, Sergio Campana, Enrico Cappellaro, Stefano Covino, Paolo D'Avanzo, Fabrizio Fiore, Dino Fugazza, Roberto Gilmozzi, Deborah Hunter, Kate Maguire, Elisabetta Maiorano, Paola Marziani, Nicola Masetti, Felix Mirabel, Hripsime Navasardyan, Ken'ichi Nomoto, Eliana Palazzi, Andrea Pastorello, Nino Panagia, L. J. Pellizza, Re'em Sari, Stephen Smartt, Gianpiero Tagliaferri, Masaomi Tanaka, Stefan Taubenberger, Nozomu Tominaga, Carrie Trundle, Massimo Turatto

*To whom correspondence should be addressed. E-mail: mazzali@mpa-garching.mpg.de

Published 24 July 2008 on *Science* Express
DOI: 10.1126/science.1158088

This PDF file includes:

Mazzali et al.

A helium-rich, energetic supernova associated with the X-ray flare XRF080109

Supplementary Information

1 Optical and infrared observations

SN 2008D was observed photometrically and spectroscopically with a number of telescopes.

Low-resolution spectra of SN 2008D have been obtained with the European Southern Observatory (ESO) 8.2m Very Large Telescope (VLT)-UT2, equipped with FORS2; the 4.2m William Herschel Telescope (WHT) equipped with ISIS; the 3.6m Telescopio Nazionale Galileo (TNG), equipped with DOLORES for optical observations and with NICS for near-IR observations; the 3.6m ESO-New Technology Telescope (NTT), equipped with EMMI; the 2.5m Nordic Optical Telescope (NOT), equipped with ALFOSC; the 2.2m Calar Alto telescope (CA), equipped with CAFOS; the 2.0m Liverpool Telescope (LT), equipped with RATCam; the 1.82m Asiago-Ekar telescope (As1.82m), equipped with AFOSC; the 0.60m Rapid Eye Mount telescope (REM), equipped with ROSS for optical observations and with REMIR for near-IR observations.

Tables S1 and S2 report the log of the observations covering the first month after the XRF, with details on the acquisition, and the photometric results. Column 1 gives the observation date, Column 2 the telescope and instrument used, Column 3 the observing setup, Column 4 the average seeing during the photometric acquisition (Table S1) and the spectral resolution (Table S2), Column 5 the observed V magnitude (Table S1) and the spectrophotometric standard used to calibrate the spectra (Table S2). The photometric errors are 1σ uncertainties.

Monochromatic light curves are shown in Fig. S1, and the spectral evolution in Fig. 2 in the main paper).

Supplementary Table S1: Photometric observations of SN 2008D

Date (2008 UT)	Telescope+ Instrument	Setup	Seeing (arcsec)	V
7.005 Jan	As1.82m+AFOSC	UBVRI	2.0	< 19.0
10.012 Jan	As1.82m+AFOSC	UBVRI	2.5	19.10 ± 0.06
11.213 Jan	TNG+NICS	JHK	0.9	–
12.168 Jan	NOT+ALFOSC	UBVRI	2.0	18.41 ± 0.10
13.006 Jan	TNG+NICS	JHK	0.8	–
13.212 Jan	TNG+DOLORES	UBVRI	0.9	18.49 ± 0.05
14.174 Jan	NOT+ALFOSC	UBVRI	1.6	18.29 ± 0.05
16.205 Jan	LT+RATCam	UBVRI	1.9	18.03 ± 0.04
17.270 Jan	LT+RATCam	UBVRI	1.6	17.96 ± 0.02
18.267 Jan	LT+RATCam	UBVRI	1.9	17.79 ± 0.04
20.024 Jan	LT+RATCam	UBVRI	2.2	17.64 ± 0.06
20.153 Jan	REM+REMIR	H	3.5	–
21.310 Jan	REM+REMIR	H	2.9	–
22.309 Jan	REM+REMIR	H	2.9	–
23.123 Jan	REM+REMIR	JK	1.4	–
25.197 Jan	VLT+FORS2	BVRI	1.0	17.36 ± 0.04
25.906 Jan	LT+RATCam	UBVRI	1.9	17.36 ± 0.03
28.021 Jan	CA+CAFOSC	UBVRI	1.2	17.33 ± 0.05
28.987 Jan	TNG+NICS	JHK	1.4	–
29.128 Jan	LT+RATCam	UBVRI	1.2	17.34 ± 0.03
30.127 Jan	LT+RATCam	UBVRI	2.9	17.35 ± 0.04
31.239 Jan	REM+ROS+REMIR	RJHK	3.0	–
31.947 Jan	TNG+NICS	JHK	3.1	–
31.964 Jan	LT+RATCam	UBVRI	1.3	17.38 ± 0.05

Supplementary Table S1: Photometric observations of SN 2008D, continued

Date (2008 UT)	Telescope+ Instrument	Setup	Seeing (arcsec)	V
01.160 Feb	LT+RATCam	UBVRI	1.3	17.43 ± 0.03
05.111 Feb	REM+ROS+REMIR	RJHK	3.2	–
06.114 Feb	LT+RATCam	BVRI	1.3	17.58 ± 0.04
08.162 Feb	LT+RATCam	UBVRI	2.1	17.74 ± 0.03
11.091 Feb	TNG+DOLORES	UBVRI	1.8	18.05 ± 0.04
13.091 Feb	REM+ROS+REMIR	JK	3.2	–

Supplementary Table S2: Spectroscopic observations of SN 2008D

Date (2008 UT)	Telescope+ Instrument	Setup	Resolution (Å)	standard
11.097 Jan	TNG+DOLORES	LR-B	12	HD93521
12.045 Jan	NOT+ALFOSC	gm4	14	Feige34
13.056 Jan	TNG+NICS	IJ	7	Hip10559
13.187 Jan	TNG+DOLORES	LR-R	13	Feige34
13.392 Jan	VLT+FORS2	300V; 300I	10	HILT600
14.194 Jan	NOT+ALFOSC	gm4	14	G191-B2B
14.944 Jan	TNG+DOLORES	LR-B	13	Feige34
16.280 Jan	VLT+FORS2	300V; 300I	10	LTT3864
25.212 Jan	VLT+FORS2	300V-300I	10	HILT600
28.033 Jan	CA+CAFOSC	b200	13	Feige34
28.270 Jan	NTT+EMMI	gm2	12	Feige34
28.935 Jan	TNG+NICS	IJ+HK	7	Hip10559
28.966 Jan	As1.82m+AFOSC	gm4+gm2	25	Feige34
29.958 Jan	As1.82m+AFOSC	gm4+gm2	25	Feige34
31.957 Jan	TNG+NICS	IJ+HK	7	Hip10559
01.002 Jan	WHT+ISIS	R300B+R158R	10	HD93521
04.107 Feb	TNG+DOLORES	LR-B+LR-R	12	Feige34
11.100 Feb	TNG+DOLORES	LR-B+LR-R	11	G191-B2B
12.185 Feb	CA+CAFOSC	b200	13	Feige34

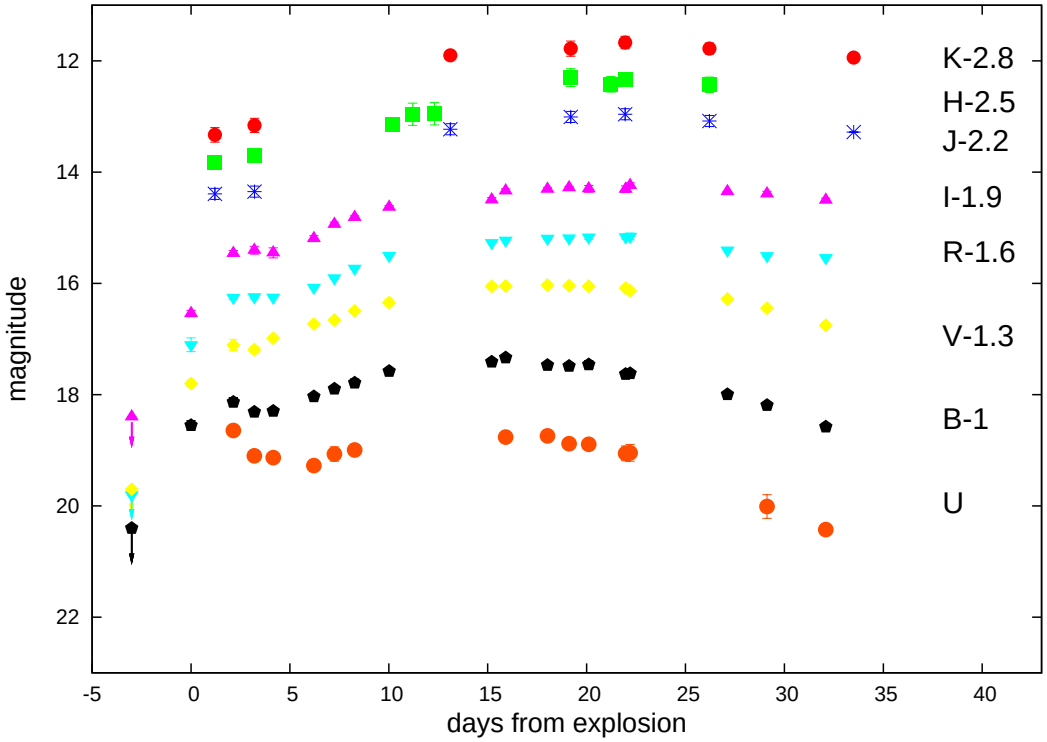

Figure 1: The monochromatic light curves of SN 2008D.

2. The properties of NGC 2770, the host of SN 2008D/XRF080109.

NGC 2770 is an Sc galaxy of luminosity class III-IV, similar to the Milky Way (S1), and very different from the hosts of long GRBs(S2). Its nucleus is rather diffuse, and according to FIRST radio maps it does not coincide with any radio peak. The SDSS spectrum of the nucleus is typical of star-forming nuclei of late-type spiral galaxies: relatively narrow lines (FWHM $< 200\,\mathrm{km\,s^{-1}}$) and diagnostic emission line ratios are consistent with photoionization by hot stars. A ratio [O III]λ5007/H$\beta = 0.68$, uncorrected because of the clearly visible Hβ absorption, makes NGC 2770 a galaxy with an H II nuclear spectrum(S3). Since the Balmer lines are mainly due to photoionization by hot stars, the star formation rate can be estimated from indicators such as the Hα flux ($0.2 M_\odot\,\mathrm{yr^{-1}}$), IRAS fluxes ($0.45 M_\odot\,\mathrm{yr^{-1}}$), or the radio luminosity at 1.4 GHz ($0.7 M_\odot\,\mathrm{yr^{-1}}$). From the FIR Luminosity we derive(S4) a SN rate $\sim 0.01\,\mathrm{SNe\,yr^{-1}}$. These values indicate that NGC 2770 does not have a very high star formation luminosity. There is no strong evidence of a hidden non-thermal source, even at radio frequencies, as already shown by ref. S5, who failed to find a high surface brightness nuclear radio source in NGC 2770.

3. Estimate of the reddening to SN 2008D and derivation of the bolometric light curve.

We estimate dust extinction towards SN 2008D from spectral comparison with other SNe Ibc. Using $E(B-V) = 0.16$ for SN 1983N (S6), an extinction $E(B-V)_{\rm tot} = 0.65$ mag for SN 2008D makes the two SNe almost identical (Fig. 3 in the main paper). This value is confirmed by two independent checks: 1) it is compatible with the neutral hydrogen column density $6 \cdot 10^{21}$ cm^{-2} estimated from X-ray spectral fits assuming a Galactic gas-to-dust ratio (7); 2) it yields optical and infrared colour light curves similar to those of other SNe Ib/c. Considering the uncertainties, we adopt for SN 2008D $E(B-V)_{tot} = 0.65 \pm 0.15$. Most of the extinction occurs in the host galaxy, since Galactic extinction is very weak [$E(B-V)_{\rm Gal} = 0.02$ mag; ref. 8].

We computed the bolometric light curve using the data in Table 1 together with the measurements reported in refs. 9 and 10.

4. X-ray data and models

The XRT light curve (Figure S2, top panel) was fitted with a function CountRate $= N(t - t_0) \sim e^{-\alpha(t-t_0)}$, where $N = 14.5 \pm 2.2$ and $\alpha = 1.09 \pm 0.13$, yielding χ^2/d.o.f. $= 13.1/16$. From this fit, the onset of the XRF can be estimated to have occurred on $JD = 2454475.06413$. The X-ray flux reaches maximum in ≈ 92 s, with an uncertainty of ~ 30 s. The decaying part of the X-ray curve can also be fitted with a power-law with index $\alpha = 1.52 \pm 0.16$. The number of photons is too small to perform time-resolved spectroscopy. Instead, we show the time evolution of the hardness ratio $HR = CR(1.5 - 10\,\mathrm{keV})/CR(0.3 - 1.5\,\mathrm{keV}$ (Fig. S2, bottom panel). The spectrum hardens during the rise to maximum and softens afterwards, a typical behaviour of X-ray flares in GRBs and in FRED profiles.

The source is affected by pile-up only within a 3-pixel radius. Therefore we extracted the photons from an annular region with a 3-pixel inner radius and a 30-pixel outer radius, yielding a total of 539 photons.

The spectrum can be fitted with a simple power-law typical of GRBs, with photon index $\Gamma = 2.29^{+0.26}_{-0.24}$ and a host galaxy hydrogen column density of $N_H = 6.42^{+1.42}_{-1.18} \cdot 10^{21}\,\mathrm{cm}^{-2}$ (χ^2/d.o.f. $= 21.1/23$). Alternatively, a model with a black body with temperature $kT = 0.20^{+0.30}_{-0.20}$ keV superimposed on a power-law with photon index $\Gamma = 2.21^{+0.48}_{-0.93}$, and a host galaxy hydrogen column density $N_H = 6.96^{+7.03}_{-2.71} \cdot 10^{21}\,\mathrm{cm}^{-2}$ yields χ^2/d.o.f. $= 20.6/21$. The total intensity is 1.85×10^{-10} erg cm^{-2} s^{-1}, and the black body intensity is no more than 14% of it, thus the presence of a black body remains uncertain (11).

The X-ray luminosity can be computed using the conversion from count rate to flux $1\,\mathrm{count\,s}^{-1}$ $= 1.17 \cdot 10^{-10}\,\mathrm{erg\ cm}^{-2}\ \mathrm{s}^{-1}$, derived from the spectral power-law fit corrected for N_H absorption. Over the 605 sec of the X-ray event, after applying a PSF correction factor of 1.88, this yields a fluence of $1.1 \cdot 10^{-7}$ erg cm^{-2}, corresponding to a total energy $1.3 \cdot 10^{46}$ erg. The peak luminosity is $\sim 8 \cdot 10^{43}$ erg s^{-1}. Assuming that the black-body component is a constant fraction (14%) of the total luminosity at any time, its luminosity, combined with the high black-body temperature ($3.8 \cdot 10^6$ K), implies an emitting radius $R_{\mathrm{ph}} \sim 10^{10}$ cm, an order of magnitude smaller than the size of Wolf-Rayet stars.

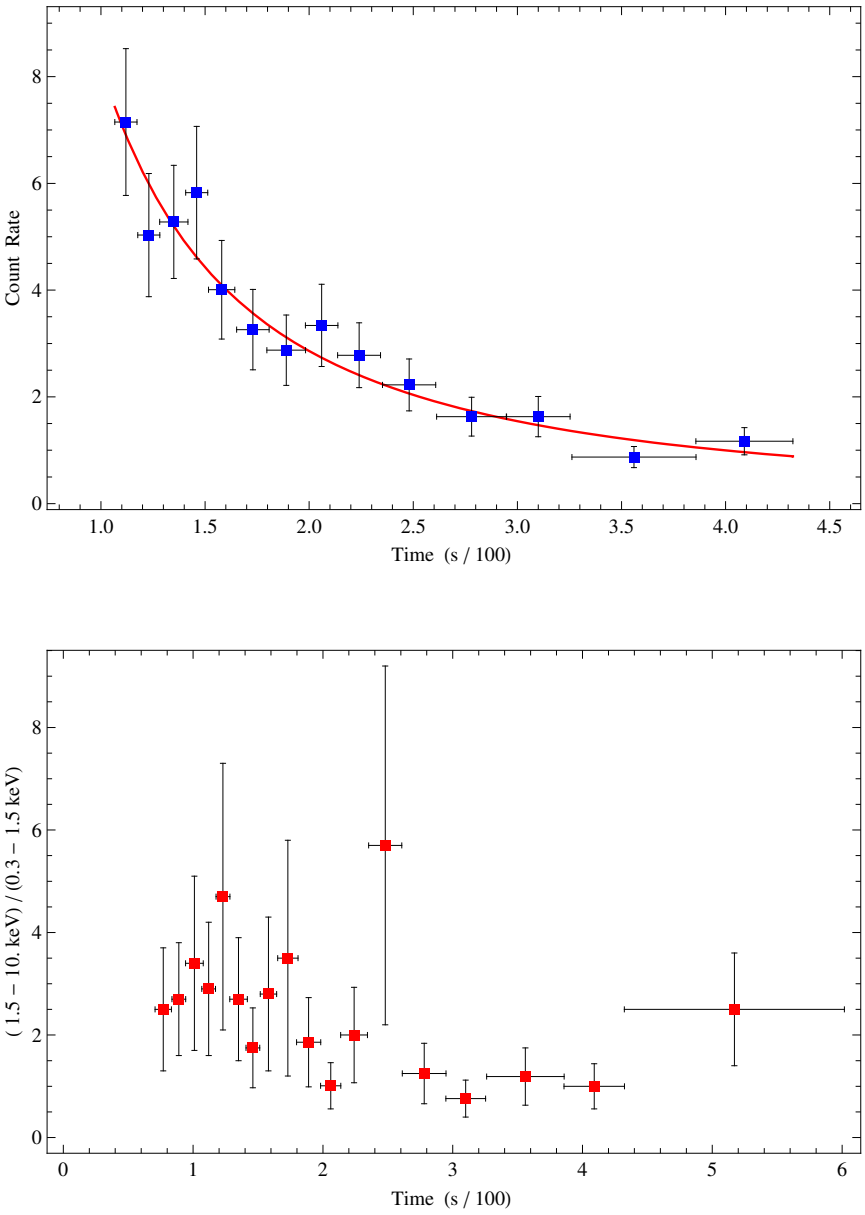

Figure 2: Top: the decaying part of the X-ray curve and a fit with a power-law with index $\alpha = 1.52 \pm 0.16$; Bottom: time evolution of the hardness ratio $HR = CR(1.5 - 10\,\mathrm{keV})/CR(0.3 - 1.5\,\mathrm{keV})$.

5. Spectral modelling.

To estimate the physical parameters that describe the supernova explosion we construct a series of radiative transfer models to derive synthetic spectra. As time elapses after the explosion of the supernova the ejecta expand and become diluted, progressively exposing deeper layers. Modelling the spectra as they evolve enables us to infer the structure of the ejected material. Among the parameters that can be determined in this way are the luminosity, the postion of the momentary photosphere, and the composition and velocity of the line-forming layers of the ejecta at each epoch.

For the spectral models we use a Monte Carlo radiative transfer code (S12, S13, S14). The code employs an approximate description of non-LTE suitable for the analysis of supernova spectra during the photospheric epochs while retaining physically meaningful relationships between model parameters. Here we use a version of the code that uses a depth-dependent composition structure (S15). For all models in the series a density structure $\rho(v)$ is adopted (for SNe a Hubble-like expansion law $r = v \cdot t$ allows us to use the ejecta velocity as a time-independent radial variable). Input parameters for each individual model are the luminosity at the given epoch, a lower boundary velocity, and the composition above this velocity. This lower boundary represents the pseudo-photosphere from which all radiation is assumed to emerge, which is a good approximation at early times. Lacking self-consistent explosion models we use a parameterized density structure which we constrain iteratively with the help of light curve and spectral models. Our model does not take into account non-thermal excitation and ionization by fast particles from the radioactive decay of ^{56}Ni. This is a fair approximation for most elements but it fails for helium. Because of the high ionization potential of He I, non-thermal processes are the main contribution to the excitation of this elements. Therefore, we cannot self-consistently derive the opacity of He I lines, which would anyway require a detailed model of the distribution of ^{56}Ni and of the geometry of the ejecta.

The very broad line features at early epochs, up to day 5 after explosion, indicate the presence of appreciable amounts of matter at high velocities above $v \sim 30,000\,\mathrm{km\,s^{-1}}$. Starting approximately 2008 January 15, ($t = 6\,\mathrm{d}$) the lines become narrower and the blue-shifted high-velocity components disappears. This suggests a significant steepening of the density gradient at lower velocities. The last spectrum considered here was obtained on 2008 February 11 ($t = 33\,\mathrm{d}$). For this model we use a lower boundary velocity of $7500\,\mathrm{km\,s^{-1}}$. The line widths of this last spectrum suggest that the density gradient

flattens below a velocity of about $9000\,\mathrm{km\,s^{-1}}$. Deeper layers are not yet accessible to observations. Fig. S3 shows the time evolution of the photospheric velocity.

A rough estimate of the parameters is obtained from the similarity of SN 2008D to SNe 2002ap and 2006aj at the earliest times and to SN 1994I at later phases. The models of these objects (S16, S17, and S18) are used as a guideline. The evolution of synthetic spectra is shown in Fig. S4.

For the models shown here we use a broken power-law with a power-law index of $n = -2.0$ in the region inside of $9000\,\mathrm{km\,s^{-1}}$, $n = -7.5$ between $9000\,\mathrm{km\,s^{-1}}$ and $17{,}000\,\mathrm{km\,s^{-1}}$, and $n = -5.5$ above $17{,}000\,\mathrm{km\,s^{-1}}$. We set the absolute density to match the observed spectral features, and obtain a total ejected mass of $\sim 7M_\odot$ with a kinetic energy of $\sim 6 \times 10^{51}\,\mathrm{erg}$, of which a mass $\sim 0.03M_\odot$ with a $E\sim 5 \times 10^{50}\,\mathrm{erg}$ is located at $v > 30{,}000\,\mathrm{km\,s^{-1}}$.

The first spectrum we consider here was taken on 12 January, 3 days after the explosion. An interesting feature of the spectra is the absence of a strong O I absorption at $\sim$ 7300 Å. The O I lines at 7774 Å that are normally responsible for this feature are very strong. Therefore we can only accommodate small amounts of oxygen in the outer layers of the ejecta. At early epochs oxygen could be so highly ionized that O I lines disappear, but the presence of Ca II and Fe II in the spectra makes this hypothesis unlikely because those species should not be present in an environment where oxygen is mostly ionized.

Overall, we can model the spectra with only a mild variation of the composition with depth. Spectra before maximum exhibit broad but shallow features of Ca, Si, and Fe-group elements suggesting the presence of only small amounts of absorbing material. In the outer part of the ejecta above $v \sim 14{,}000\,\mathrm{km\,s^{-1}}$ we assume a composition dominated by He. The attenuation of the flux in the blue requires the presence of some Ti and other Fe-group elements that do not produce strong individual line features but block radiation in the blue and UV through a large number of overlapping weaker lines.

At epochs around and after maximum the spectra show distinctly narrower line features that can be attributed the He I, O I, Ca II and Fe II. There is also some indication for C I in the red and infrared region (S19). In the inner part we assume a composition where C and O dominate with a slightly enhanced contribution from heavy elements, likely including some decay products of radioactive ^{56}Ni.

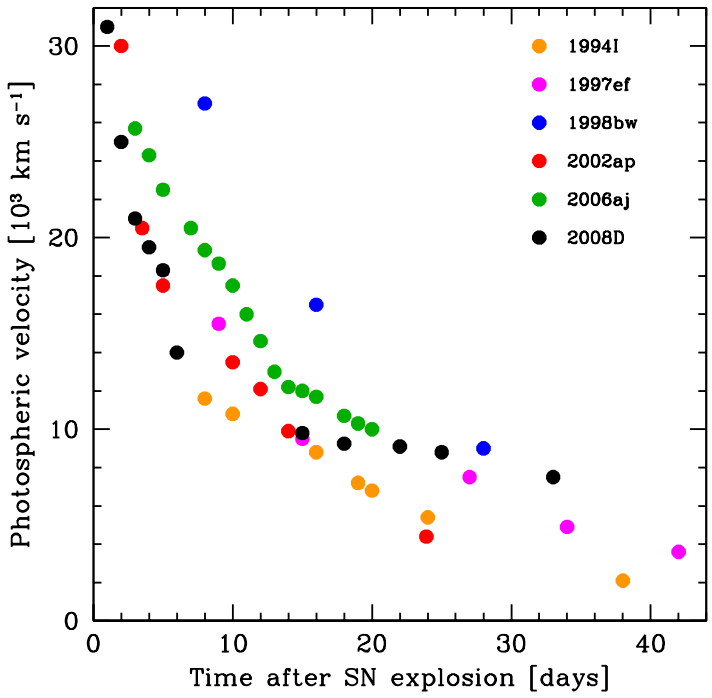

Figure 3: The temporal evolution of the lower boundary (photosphere) velocity used in the models for SN 2008D compared to the cases of other SNe Ic. SN 2008D starts out with a very high velocity, like SN 2002ap, then transitions to lower velocities like SN 1994I. This is the phase when broad lines disappear. At later times the evolution is slower than that of SN 1994I, indicating a large mass with a small density gradient in the inner layers, similar to SN 1997ef. Only SNe with velocities larger than SNe 2008D or 2002ap were accompanied by a GRB or an XRF.

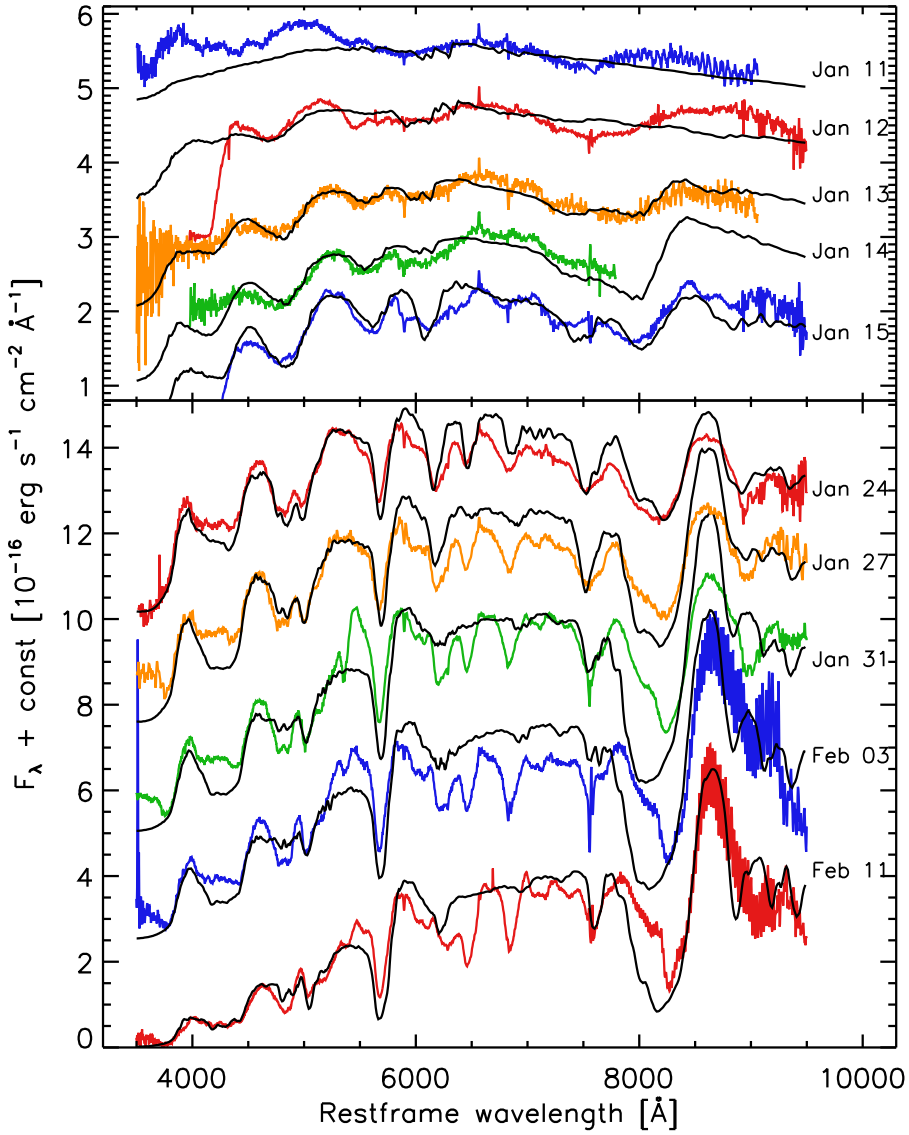

Figure 4: Series of model spectra for the sequence of early time spectra of SN 2008D. The optical depth in He I lines in the model of 24 January has been enhanced to mimic the effect of non-thermal excitations by fast electrons generated in the decay of ^{56}Ni. While we cannot constrain the abundance of He this way this method allows us to identify He lines in the spectrum. The first two spectra are contaminated by the emission of the afterglow which is not described by the model. Therefore, the luminosity needed to match those spectra is too high to give a consistent description leading to an over-ionization of most species. This affects in particularly the Ca II IR triplet near 8000 Å, which is not reproduced by the models in the first two epochs.

References.

1. van den Bergh, S., Li, W., & Filippenko, A. V. *Pub. Astron. Soc. Pac.*, 115, 1280 (2003).

2. Fruchter, A., et al. , *Nature*441, 463-468 (2006).

3. Veilleux, S., & Osterbrock, D. E. , *Astroph. J. Suppl.*, 63, 295 (1987).

4. Mannucci, F., et al. , *Astron. Astrophys.*, 401, 519 (2003).

5. Ulvestad, J. S., & Ho, L. C. *Astroph. J.*, 581, 925 (2002).

6. Clocchiatti, A., & Wheeler, J.C. *Astroph. J.*, 491, 375 (1997).

7. Page, K.L., *et al.* GCN 7164 (2008).

8. Schlegel, D.J., Finkbeiner, D.P., & Davis, M., *Astroph. J.*, 500, 525 (1998).

9. Immler, S., et al. GRB Coordinates Network, 7168, 1 (2008).

10. Li, W., Chornock, R., Foley, R. J., Filippenko, A. V., Modjaz, M., Poznanski, D., & Bloom, J. S. GRB Coordinates Network, 7176, 1 (2008).

11. Li, L.-X., astro-ph 0803.0079 (2008).

12. Mazzali, P. A. & Lucy, L. B., *Astron. Astrophys.*, 279, 447 (1993).

13. Lucy, L. B., *Astron. Astrophys.*, 345, 211 (1999).

14. Mazzali, P. A., *Astron. Astrophys.*, 363, 705 (2000).

15. Stehle, M., Mazzali, P. A., Benetti, S., & Hillebrandt, W., *Monthly Not. Roy. Astron. Soc.*, 360, 1231 (2005).

16. Mazzali, P. A., et al., *Astroph. J. Letters*, 572, L61 (2002).

17. Mazzali, P. A., et al., *Nature*, 442, 1018 (2006).

18. Sauer, D. N., et al., *Monthly Not. Roy. Astron. Soc.*, 369, 1939 (2006).

19. Valenti, S., et al., *Astroph. J. Letters*, 673, L155 (2008).